Fermilab-Pub-11/052-E

Measurement of spin correlation in $t\bar{t}$ production using dilepton final states

V.M. Abazov,[35] B. Abbott,[73] B.S. Acharya,[29] M. Adams,[49] T. Adams,[47] G.D. Alexeev,[35] G. Alkhazov,[39] A. Alton[a],[61] G. Alverson,[60] G.A. Alves,[2] L.S. Ancu,[34] M. Aoki,[48] M. Arov,[58] A. Askew,[47] B. Åsman,[41] O. Atramentov,[65] C. Avila,[8] J. BackusMayes,[80] F. Badaud,[13] L. Bagby,[48] B. Baldin,[48] D.V. Bandurin,[47] S. Banerjee,[29] E. Barberis,[60] P. Baringer,[56] J. Barreto,[3] J.F. Bartlett,[48] U. Bassler,[18] V. Bazterra,[49] S. Beale,[6] A. Bean,[56] M. Begalli,[3] M. Begel,[71] C. Belanger-Champagne,[41] L. Bellantoni,[48] S.B. Beri,[27] G. Bernardi,[17] R. Bernhard,[22] I. Bertram,[42] M. Besançon,[18] R. Beuselinck,[43] V.A. Bezzubov,[38] P.C. Bhat,[48] V. Bhatnagar,[27] G. Blazey,[50] S. Blessing,[47] K. Bloom,[64] A. Boehnlein,[48] D. Boline,[70] T.A. Bolton,[57] E.E. Boos,[37] G. Borissov,[42] T. Bose,[59] A. Brandt,[76] O. Brandt,[23] R. Brock,[62] G. Brooijmans,[68] A. Bross,[48] D. Brown,[17] J. Brown,[17] X.B. Bu,[48] M. Buehler,[79] V. Buescher,[24] V. Bunichev,[37] S. Burdin[b],[42] T.H. Burnett,[80] C.P. Buszello,[41] B. Calpas,[15] E. Camacho-Pérez,[32] M.A. Carrasco-Lizarraga,[56] B.C.K. Casey,[48] H. Castilla-Valdez,[32] S. Chakrabarti,[70] D. Chakraborty,[50] K.M. Chan,[54] A. Chandra,[78] G. Chen,[56] S. Chevalier-Théry,[18] D.K. Cho,[75] S.W. Cho,[31] S. Choi,[31] B. Choudhary,[28] T. Christoudias,[43] S. Cihangir,[48] D. Claes,[64] J. Clutter,[56] M. Cooke,[48] W.E. Cooper,[48] M. Corcoran,[78] F. Couderc,[18] M.-C. Cousinou,[15] A. Croc,[18] D. Cutts,[75] A. Das,[45] G. Davies,[43] K. De,[76] S.J. de Jong,[34] E. De La Cruz-Burelo,[32] F. Déliot,[18] M. Demarteau,[48] R. Demina,[69] D. Denisov,[48] S.P. Denisov,[38] S. Desai,[48] K. DeVaughan,[64] H.T. Diehl,[48] M. Diesburg,[48] A. Dominguez,[64] T. Dorland,[80] A. Dubey,[28] L.V. Dudko,[37] D. Duggan,[65] A. Duperrin,[15] S. Dutt,[27] A. Dyshkant,[50] M. Eads,[64] D. Edmunds,[62] J. Ellison,[46] V.D. Elvira,[48] Y. Enari,[17] H. Evans,[52] A. Evdokimov,[71] V.N. Evdokimov,[38] G. Facini,[60] T. Ferbel,[69] F. Fiedler,[24] F. Filthaut,[34] W. Fisher,[62] H.E. Fisk,[48] M. Fortner,[50] H. Fox,[42] S. Fuess,[48] T. Gadfort,[71] A. Garcia-Bellido,[69] V. Gavrilov,[36] P. Gay,[13] W. Geist,[19] W. Geng,[15,62] D. Gerbaudo,[66] C.E. Gerber,[49] Y. Gershtein,[65] G. Ginther,[48,69] G. Golovanov,[35] A. Goussiou,[80] P.D. Grannis,[70] S. Greder,[19] H. Greenlee,[48] Z.D. Greenwood,[58] E.M. Gregores,[4] G. Grenier,[20] Ph. Gris,[13] J.-F. Grivaz,[16] A. Grohsjean,[18] S. Grünendahl,[48] M.W. Grünewald,[30] T. Guillemin,[16] F. Guo,[70] G. Gutierrez,[48] P. Gutierrez,[73] A. Haas[c],[68] S. Hagopian,[47] J. Haley,[60] L. Han,[7] K. Harder,[44] A. Harel,[69] J.M. Hauptman,[55] J. Hays,[43] T. Head,[44] T. Hebbeker,[21] D. Hedin,[50] H. Hegab,[74] A.P. Heinson,[46] U. Heintz,[75] C. Hensel,[23] I. Heredia-De La Cruz,[32] K. Herner,[61] G. Hesketh[d],[44] M.D. Hildreth,[54] R. Hirosky,[79] T. Hoang,[47] J.D. Hobbs,[70] B. Hoeneisen,[12] M. Hohlfeld,[24] Z. Hubacek,[10,18] N. Huske,[17] V. Hynek,[10] I. Iashvili,[67] R. Illingworth,[48] A.S. Ito,[48] S. Jabeen,[75] M. Jaffré,[16] D. Jamin,[15] A. Jayasinghe,[73] R. Jesik,[43] K. Johns,[45] M. Johnson,[48] D. Johnston,[64] A. Jonckheere,[48] P. Jonsson,[43] J. Joshi,[27] A. Juste,[40] K. Kaadze,[57] E. Kajfasz,[15] D. Karmanov,[37] P.A. Kasper,[48] I. Katsanos,[64] R. Kehoe,[77] S. Kermiche,[15] N. Khalatyan,[48] A. Khanov,[74] A. Kharchilava,[67] Y.N. Kharzheev,[35] D. Khatidze,[75] M.H. Kirby,[51] J.M. Kohli,[27] A.V. Kozelov,[38] J. Kraus,[62] S. Kulikov,[38] A. Kumar,[67] A. Kupco,[11] T. Kurča,[20] V.A. Kuzmin,[37] J. Kvita,[9] S. Lammers,[52] G. Landsberg,[75] P. Lebrun,[20] H.S. Lee,[31] S.W. Lee,[55] W.M. Lee,[48] J. Lellouch,[17] L. Li,[46] Q.Z. Li,[48] S.M. Lietti,[5] J.K. Lim,[31] D. Lincoln,[48] J. Linnemann,[62] V.V. Lipaev,[38] R. Lipton,[48] Y. Liu,[7] Z. Liu,[6] A. Lobodenko,[39] M. Lokajicek,[11] R. Lopes de Sa,[70] H.J. Lubatti,[80] R. Luna-Garcia[e],[32] A.L. Lyon,[48] A.K.A. Maciel,[2] D. Mackin,[78] R. Madar,[18] R. Magaña-Villalba,[32] S. Malik,[64] V.L. Malyshev,[35] Y. Maravin,[57] J. Martínez-Ortega,[32] R. McCarthy,[70] C.L. McGivern,[56] M.M. Meijer,[34] A. Melnitchouk,[63] D. Menezes,[50] P.G. Mercadante,[4] M. Merkin,[37] A. Meyer,[21] J. Meyer,[23] F. Miconi,[19] N.K. Mondal,[29] G.S. Muanza,[15] M. Mulhearn,[79] E. Nagy,[15] M. Naimuddin,[28] M. Narain,[75] R. Nayyar,[28] H.A. Neal,[61] J.P. Negret,[8] P. Neustroev,[39] S.F. Novaes,[5] T. Nunnemann,[25] G. Obrant,[39] J. Orduna,[78] N. Osman,[15] J. Osta,[54] G.J. Otero y Garzón,[1] M. Padilla,[46] A. Pal,[76] M. Pangilinan,[75] N. Parashar,[53] V. Parihar,[75] S.K. Park,[31] J. Parsons,[68] R. Partridge[c],[75] N. Parua,[52] A. Patwa,[71] B. Penning,[48] M. Perfilov,[37] K. Peters,[44] Y. Peters,[44] K. Petridis,[44] G. Petrillo,[69] P. Pétroff,[16] R. Piegaia,[1] J. Piper,[62] M.-A. Pleier,[71] P.L.M. Podesta-Lerma[f],[32] V.M. Podstavkov,[48] M.-E. Pol,[2] P. Polozov,[36] A.V. Popov,[38] M. Prewitt,[78] D. Price,[52] N. Prokopenko,[38] S. Protopopescu,[71] J. Qian,[61] A. Quadt,[23] B. Quinn,[63] M.S. Rangel,[2] K. Ranjan,[28] P.N. Ratoff,[42] I. Razumov,[38] P. Renkel,[77] M. Rijssenbeek,[70] I. Ripp-Baudot,[19] F. Rizatdinova,[74] M. Rominsky,[48] A. Ross,[42] C. Royon,[18] P. Rubinov,[48] R. Ruchti,[54] G. Safronov,[36] G. Sajot,[14] P. Salcido,[50] A. Sánchez-Hernández,[32] M.P. Sanders,[25] B. Sanghi,[48] A.S. Santos,[5] G. Savage,[48] L. Sawyer,[58] T. Scanlon,[43] R.D. Schamberger,[70] Y. Scheglov,[39] H. Schellman,[51] T. Schliephake,[26] S. Schlobohm,[80] C. Schwanenberger,[44] R. Schwienhorst,[62] J. Sekaric,[56] H. Severini,[73] E. Shabalina,[23] V. Shary,[18] A.A. Shchukin,[38] R.K. Shivpuri,[28] V. Simak,[10] V. Sirotenko,[48] P. Skubic,[73] P. Slattery,[69] D. Smirnov,[54] K.J. Smith,[67] G.R. Snow,[64] J. Snow,[72] S. Snyder,[71] S. Söldner-Rembold,[44] L. Sonnenschein,[21] K. Soustruznik,[9] J. Stark,[14] V. Stolin,[36] D.A. Stoyanova,[38] M. Strauss,[73]

D. Strom,[49] L. Stutte,[48] L. Suter,[44] P. Svoisky,[73] M. Takahashi,[44] A. Tanasijczuk,[1] W. Taylor,[6] M. Titov,[18] V.V. Tokmenin,[35] Y.-T. Tsai,[69] D. Tsybychev,[70] B. Tuchming,[18] C. Tully,[66] P.M. Tuts,[68] L. Uvarov,[39] S. Uvarov,[39] S. Uzunyan,[50] R. Van Kooten,[52] W.M. van Leeuwen,[33] N. Varelas,[49] E.W. Varnes,[45] I.A. Vasilyev,[38] P. Verdier,[20] L.S. Vertogradov,[35] M. Verzocchi,[48] M. Vesterinen,[44] D. Vilanova,[18] P. Vint,[43] P. Vokac,[10] H.D. Wahl,[47] M.H.L.S. Wang,[69] J. Warchol,[54] G. Watts,[80] M. Wayne,[54] M. Weber^{g},[48] L. Welty-Rieger,[51] A. White,[76] D. Wicke,[26] M.R.J. Williams,[42] G.W. Wilson,[56] M. Wobisch,[58] D.R. Wood,[60] T.R. Wyatt,[44] Y. Xie,[48] C. Xu,[61] S. Yacoob,[51] R. Yamada,[48] W.-C. Yang,[44] T. Yasuda,[48] Y.A. Yatsunenko,[35] Z. Ye,[48] H. Yin,[48] K. Yip,[71] S.W. Youn,[48] J. Yu,[76] S. Zelitch,[79] T. Zhao,[80] B. Zhou,[61] J. Zhu,[61] M. Zielinski,[69] D. Zieminska,[52] and L. Zivkovic[75]

(The D0 Collaboration*)

[1]*Universidad de Buenos Aires, Buenos Aires, Argentina*
[2]*LAFEX, Centro Brasileiro de Pesquisas Físicas, Rio de Janeiro, Brazil*
[3]*Universidade do Estado do Rio de Janeiro, Rio de Janeiro, Brazil*
[4]*Universidade Federal do ABC, Santo André, Brazil*
[5]*Instituto de Física Teórica, Universidade Estadual Paulista, São Paulo, Brazil*
[6]*Simon Fraser University, Vancouver, British Columbia, and York University, Toronto, Ontario, Canada*
[7]*University of Science and Technology of China, Hefei, People's Republic of China*
[8]*Universidad de los Andes, Bogotá, Colombia*
[9]*Charles University, Faculty of Mathematics and Physics, Center for Particle Physics, Prague, Czech Republic*
[10]*Czech Technical University in Prague, Prague, Czech Republic*
[11]*Center for Particle Physics, Institute of Physics, Academy of Sciences of the Czech Republic, Prague, Czech Republic*
[12]*Universidad San Francisco de Quito, Quito, Ecuador*
[13]*LPC, Université Blaise Pascal, CNRS/IN2P3, Clermont, France*
[14]*LPSC, Université Joseph Fourier Grenoble 1, CNRS/IN2P3, Institut National Polytechnique de Grenoble, Grenoble, France*
[15]*CPPM, Aix-Marseille Université, CNRS/IN2P3, Marseille, France*
[16]*LAL, Université Paris-Sud, CNRS/IN2P3, Orsay, France*
[17]*LPNHE, Universités Paris VI and VII, CNRS/IN2P3, Paris, France*
[18]*CEA, Irfu, SPP, Saclay, France*
[19]*IPHC, Université de Strasbourg, CNRS/IN2P3, Strasbourg, France*
[20]*IPNL, Université Lyon 1, CNRS/IN2P3, Villeurbanne, France and Université de Lyon, Lyon, France*
[21]*III. Physikalisches Institut A, RWTH Aachen University, Aachen, Germany*
[22]*Physikalisches Institut, Universität Freiburg, Freiburg, Germany*
[23]*II. Physikalisches Institut, Georg-August-Universität Göttingen, Göttingen, Germany*
[24]*Institut für Physik, Universität Mainz, Mainz, Germany*
[25]*Ludwig-Maximilians-Universität München, München, Germany*
[26]*Fachbereich Physik, Bergische Universität Wuppertal, Wuppertal, Germany*
[27]*Panjab University, Chandigarh, India*
[28]*Delhi University, Delhi, India*
[29]*Tata Institute of Fundamental Research, Mumbai, India*
[30]*University College Dublin, Dublin, Ireland*
[31]*Korea Detector Laboratory, Korea University, Seoul, Korea*
[32]*CINVESTAV, Mexico City, Mexico*
[33]*FOM-Institute NIKHEF and University of Amsterdam/NIKHEF, Amsterdam, The Netherlands*
[34]*Radboud University Nijmegen/NIKHEF, Nijmegen, The Netherlands*
[35]*Joint Institute for Nuclear Research, Dubna, Russia*
[36]*Institute for Theoretical and Experimental Physics, Moscow, Russia*
[37]*Moscow State University, Moscow, Russia*
[38]*Institute for High Energy Physics, Protvino, Russia*
[39]*Petersburg Nuclear Physics Institute, St. Petersburg, Russia*
[40]*Institució Catalana de Recerca i Estudis Avançats (ICREA) and Institut de Física d'Altes Energies (IFAE), Barcelona, Spain*
[41]*Stockholm University, Stockholm and Uppsala University, Uppsala, Sweden*
[42]*Lancaster University, Lancaster LA1 4YB, United Kingdom*
[43]*Imperial College London, London SW7 2AZ, United Kingdom*
[44]*The University of Manchester, Manchester M13 9PL, United Kingdom*
[45]*University of Arizona, Tucson, Arizona 85721, USA*
[46]*University of California Riverside, Riverside, California 92521, USA*
[47]*Florida State University, Tallahassee, Florida 32306, USA*
[48]*Fermi National Accelerator Laboratory, Batavia, Illinois 60510, USA*
[49]*University of Illinois at Chicago, Chicago, Illinois 60607, USA*
[50]*Northern Illinois University, DeKalb, Illinois 60115, USA*

[51]Northwestern University, Evanston, Illinois 60208, USA
[52]Indiana University, Bloomington, Indiana 47405, USA
[53]Purdue University Calumet, Hammond, Indiana 46323, USA
[54]University of Notre Dame, Notre Dame, Indiana 46556, USA
[55]Iowa State University, Ames, Iowa 50011, USA
[56]University of Kansas, Lawrence, Kansas 66045, USA
[57]Kansas State University, Manhattan, Kansas 66506, USA
[58]Louisiana Tech University, Ruston, Louisiana 71272, USA
[59]Boston University, Boston, Massachusetts 02215, USA
[60]Northeastern University, Boston, Massachusetts 02115, USA
[61]University of Michigan, Ann Arbor, Michigan 48109, USA
[62]Michigan State University, East Lansing, Michigan 48824, USA
[63]University of Mississippi, University, Mississippi 38677, USA
[64]University of Nebraska, Lincoln, Nebraska 68588, USA
[65]Rutgers University, Piscataway, New Jersey 08855, USA
[66]Princeton University, Princeton, New Jersey 08544, USA
[67]State University of New York, Buffalo, New York 14260, USA
[68]Columbia University, New York, New York 10027, USA
[69]University of Rochester, Rochester, New York 14627, USA
[70]State University of New York, Stony Brook, New York 11794, USA
[71]Brookhaven National Laboratory, Upton, New York 11973, USA
[72]Langston University, Langston, Oklahoma 73050, USA
[73]University of Oklahoma, Norman, Oklahoma 73019, USA
[74]Oklahoma State University, Stillwater, Oklahoma 74078, USA
[75]Brown University, Providence, Rhode Island 02912, USA
[76]University of Texas, Arlington, Texas 76019, USA
[77]Southern Methodist University, Dallas, Texas 75275, USA
[78]Rice University, Houston, Texas 77005, USA
[79]University of Virginia, Charlottesville, Virginia 22901, USA
[80]University of Washington, Seattle, Washington 98195, USA

(Dated: March 9, 2011)

We measure the correlation between the spin of the top quark and the spin of the anti-top quark in $t\bar{t} \to W^+bW^-\bar{b} \to \ell^+\nu b\ell^-\bar{\nu}\bar{b}$ final states produced in $p\bar{p}$ collisions at a center of mass energy $\sqrt{s} = 1.96$ TeV, where ℓ is an electron or muon. The data correspond to an integrated luminosity of 5.4 fb^{-1} and were collected with the D0 detector at the Fermilab Tevatron collider. The correlation is extracted from the angles of the two leptons in the t and $\bar{t}$ rest frames, yielding a correlation strength $C = 0.10^{+0.45}_{-0.45}$, in agreement with the NLO QCD prediction within two standard deviations, but also in agreement with the no correlation hypothesis.

PACS numbers: 14.65.Ha, 12.38.Qk, 13.85.Qk

I. INTRODUCTION

Measurements of top quark properties play an important role in testing the standard model (SM) and its possible extensions. While top and anti-top quarks are unpolarized in $t\bar{t}$ production at hadron colliders, the orientation of their spins are correlated [1]. The SM also predicts that top quarks decay before the correlation between the direction of the spin of the t and $\bar{t}$ quark can be affected by fragmentation [2]. This contrasts with the longer-lived lighter quarks, for which the spins become decorrelated by strong interactions before they decay [3]. The orientation of the spin of the top quark is therefore reflected in its decay products.

The charged leptons from the $t \to Wb \to \ell\nu_\ell b$ decays are the probes with the highest sensitivity to the direction of the t quark spin (if not stated otherwise, charge conjugated states are implied through out the paper). Therefore the final state in which both W bosons from t quarks decay to leptons, referred to as dilepton final state, is ideal for measurements of the correlation between the spins of pair-produced top and anti-top quarks and thus to test the SM [4, 5].

The observation of spin correlation as expected in the SM would indicate that the top quark decays before the spin direction is affected by its fragmentation and therefore provides an upper limit on the lifetime of the top quark. This can be related to the Cabibbo-Kobayashi-Maskawa matrix element V_{tb} without assumptions about the number of quark generations [6]. Scenarios beyond

*with visitors from [a]Augustana College, Sioux Falls, SD, USA, [b]The University of Liverpool, Liverpool, UK, [c]SLAC, Menlo Park, CA, USA, [d]University College London, London, UK, [e]Centro de Investigacion en Computacion - IPN, Mexico City, Mexico, [f]ECFM, Universidad Autonoma de Sinaloa, Culiacán, Mexico, and [g]Universität Bern, Bern, Switzerland.

the SM [2, 7–11] predict different production and decay dynamics for the top quark, which could affect the spin correlation.

There is a recent measurement of $t\bar{t}$ spin correlation in semileptonic final states, in which one W boson decays to leptons and the other to quarks, by the CDF Collaboration [12] in 4.3 fb^{-1} of $p\bar{p}$ collisions at $\sqrt{s} = 1.96$ TeV which agrees with the SM prediction. There is also an earlier measurement analyzing dilepton final states by the D0 Collaboration using an integrated luminosity of 125 pb^{-1} of $p\bar{p}$ collisions at $\sqrt{s} = 1.8$ TeV [13]. However, the expected sensitivity of both previous measurements was not high enough to distinguish between a hypothesis of no correlation and the correlation predicted in the SM. In both measurements a different sign convention than the one in this article was used [14].

In this letter, we measure the strength of the $t\bar{t}$ spin correlation C from a differential angular distribution involving the angles between the flight direction of the two decay leptons in the rest frames of their respective t quarks and the spin quantization axis (defined below). Top quarks are assumed to decay as predicted by the SM. We analyze the dilepton channels which correspond to decays of the W bosons (from t and $\bar{t}$ quark decays) into an electron and electron neutrino, a muon and a muon neutrino or a tau lepton and a tau neutrino if the tau decays leptonically. The analysis is performed using 5.4 fb^{-1} of $p\bar{p}$ collisions at $\sqrt{s} = 1.96$ TeV collected with the D0 detector at the Fermilab Tevatron collider.

To reduce the dependence on the signal normalization, we extract the spin correlation simultaneously with the $t\bar{t}$ production cross section ($\sigma_{t\bar{t}}$). In the SM, $\sigma_{t\bar{t}}$ is predicted to a precision of (6–8)% [15–19]. Many models of physics beyond the SM predict effects in the top quark sector that can affect both the top quark production rate and the spin correlation. For example, in supersymmetric models [20], pair production of scalar top quarks decaying into a b quark, an electron or muon, and a scalar neutrino [21] would affect the measured values of both $\sigma_{t\bar{t}}$ and C in dilepton final states.

II. OBSERVABLE

The $t\bar{t}$ spin correlation strength C is obtained from the distribution [5]

$$\frac{1}{\sigma}\frac{d^2\sigma}{d\cos\theta_1 d\cos\theta_2} = \frac{1}{4}(1 - C\cos\theta_1\cos\theta_2) \ , \qquad (1)$$

where σ denotes the cross section, and θ_1 and θ_2 are the angles between the direction of flight of the decay leptons ℓ^+ and ℓ^- in the t and $\bar{t}$ rest frames and the spin quantization axis [22]. These angles are chosen because the sensitivity to the spin correlation is largest when the decay products are down-type fermions [4, 5, 9]. C is a parameter between -1 and 1 that depends on the quantization axis used and determines the magnitude of the $t\bar{t}$ spin correlation. For the Tevatron, it has been shown in [5] that an almost optimal choice of quantization axis is given by the direction of the beam. At tree level in quantum chromodynamics (QCD), C represents the number of events where the t and $\bar{t}$ spins are parallel minus the number of events where they are anti-parallel, normalized by the total number of events. The case of all spins being (anti-)parallel corresponds to $C = 1$ ($C = -1$), whereas an equal mixture of parallel and anti-parallel would give $C = 0$. Choosing the beam momentum vector as the quantization axis, $C = 0.777^{+0.027}_{-0.042}$ is predicted at NLO in QCD [5]. This calculation uses the CTEQ6.1M parton distribution functions (PDF) with both the factorization and renormalization scale set to the top quark mass (m_t). The uncertainty reflects the variation of this scale from $m_t/2$ to $2m_t$. Figure 1 shows the $\cos\theta_1\cos\theta_2$ distribution calculated with spin correlation ($C = 0.777$) and without spin correlation ($C = 0$). A non-vanishing spin correlation leads to an asymmetry in the distribution.

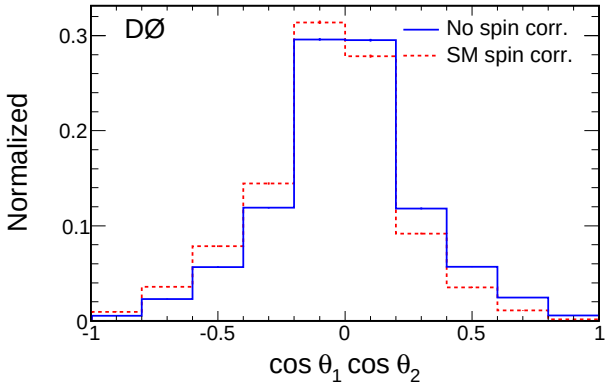

FIG. 1: The distribution in $\cos\theta_1\cos\theta_2$ for a $t\bar{t}$ sample including the NLO QCD spin correlation ($C = 0.777$) (dashed line) and with no spin correlation ($C = 0$) (solid line) at the parton level, generated using MC@NLO [23].

III. D0 DETECTOR

The D0 detector [24] contains a tracking system, a calorimeter, and a muon spectrometer. The tracking system consists of a silicon microstrip tracker (SMT) and a central fiber tracker, both located inside a 1.9 T superconducting solenoid. The design provides efficient charged-particle tracking in the pseudorapidity region $|\eta_{\rm det}| < 3$ [25]. The SMT provides the capability of reconstructing the $p\bar{p}$ interaction vertex (PV) with a precision of about 40 μm in the plane transverse to the beam direction and a determination of the impact parameter of any track relative to the PV [26] with a precision between 20 and 50 μm, depending on the number of hits in the

SMT. The calorimeter has a central section (CC) covering $|\eta_{\rm det}| < 1.1$ and two end calorimeters (EC) extending coverage to $|\eta_{\rm det}| \approx 4.2$. The muon system surrounds the calorimeter and consists of three layers of tracking detectors and of scintillators covering $|\eta_{\rm det}| < 2$ [27]. A 1.8 T toroidal iron magnet is located outside the innermost layer of the muon detector. The luminosity is calculated from the rate of $p\bar{p}$ inelastic collisions, measured with plastic scintillator arrays which are located in front of the EC cryostats.

The D0 trigger is based on a three-level pipeline system. The first level consists of hardware and firmware components, the second level combines information from different detectors to construct simple physical quantities, while the software-based third level processes the full event information using simplified reconstruction algorithms [28].

IV. EVENT SELECTION

The selections for the $\ell\ell$ (ee, $e\mu$, and $\mu\mu$) decay channels follow those described in Ref. [29]. Electrons are defined as clusters of calorimeter cells for which: (i) the energy deposited in the electromagnetic section of the calorimeter is $> 90\%$ of the total cluster energy, (ii) the energy is concentrated in a narrow cone and is isolated from other energy depositions, (iii) the spatial distribution of the shower is compatible with that of an electron and matches a track emanating from the PV. To further reduce background, we use the tracking system and calorimeter information to form a likelihood discriminant that enhances the efficiency to select real and to reject fake electrons. Electrons that fulfill criteria (i) to (iii) are referred to as "loose" electrons, while those that also fulfill the likelihood criterion are referred to as "tight" electrons. Both central ($|\eta_{\rm det}| < 1.1$) and forward ($1.5 < |\eta_{\rm det}| < 2.5$) electrons are considered in the analysis.

Muons are defined using tracks reconstructed in the three layers of the muon system, with a matching track found in the central tracking system. To reduce background, the sum of the track p_T in a cone of size $\mathcal{R} = \sqrt{(\Delta y)^2 + (\Delta\phi)^2} = 0.5$ around the muon axis must be $< 15\%$ of the muon p_T. We also require the sum of calorimeter cell energies in an annulus of radius $0.1 < \Delta\mathcal{R} < 0.4$ relative to the axis of the muon track to be $< 15\%$ of the muon p_T. Muon candidates originating from top quark decays are required to have a distance of closest approach of the muon track with respect to the PV < 0.2 cm for a muon track without a hit in the SMT, and < 0.02 cm for a muon track with a hit in the SMT. Furthermore, muons must satisfy $|\eta_{\rm det}| < 2$.

Jets are reconstructed with a mid-point cone algorithm [30] with radius $\mathcal{R} = 0.5$. Jet energies are corrected for calorimeter response, additional energy from noise, pileup, and multiple $p\bar{p}$ interactions in the same bunch crossing, and out-of-cone shower development in the calorimeter.

Jets are required to contain three or more tracks originating from the PV within each jet cone. The high instantaneous luminosity achieved by the Tevatron leads to a significant background contribution from additional $p\bar{p}$ collisions within the same bunch crossing. The track requirement removes jets from such collisions and is only necessary for data taken after the initial 1 fb^{-1} data set. The missing transverse energy ($\not\!\!E_T$) is defined by the magnitude and direction opposite to the vector sum of all significant transverse energies deposited in calorimeter cells. The transverse energy of muons and corrections made to electron and jet energies are taken into account. A more detailed description of object reconstruction can be found in [31].

To select top quark pair events, we require two isolated, oppositely charged leptons with $p_T > 15$ GeV for all channels. At least two jets with $p_T > 20$ GeV and $|\eta_{\rm det}| < 2.5$ are required. The final selection in the $e\mu$ channel requires that H_T (defined as the scalar sum of the leading lepton p_T and the p_T of each of the two most energetic jets) be greater than 110 GeV. This requirement allows rejection of the largest backgrounds for this final state arising from $Z/\gamma^* \to \tau^+\tau^-$ and diboson production. To further reject Z/γ^* background, where $\not\!\!E_T$ arises from mismeasurement, we compute for each ee and $\mu\mu$ event a $\not\!\!E_T$ significance likelihood based on the $\not\!\!E_T$ probability distribution calculated from the $\not\!\!E_T$ and the lepton and jet energy resolutions. We require this quantity to exceed 5. We find that only in the $\mu\mu$ channel an additional cut on missing transverse energy is beneficial to increase the signal purity, and therefore require $\not\!\!E_T > 40$ GeV for $\mu\mu$ final states.

V. SIGNAL AND BACKGROUND MODELING

Signal and background processes are modeled with a combination of Monte Carlo (MC) simulation and data. Top quark pair production is simulated using the MC@NLO [23] generator assuming $m_t = 172.5$ GeV. Events are processed through HERWIG [32] to simulate fragmentation, hadronization and decays of short-lived particles. We generate $t\bar{t}$ MC samples both with and without the expected spin correlation, as both options are available in MC@NLO. To cross check, we also use the ALPGEN [33] matrix-element generator interfaced to PYTHIA [34] to simulate parton showering. In all three cases events are processed through a full detector simulation using GEANT [35]. The MC events are overlaid with data events from random bunch crossings to model the effects of detector noise and additional $p\bar{p}$ interactions. The same reconstruction programs are then applied to data and MC events. Lepton trigger and identification efficiencies as well as lepton momentum resolutions are derived from $Z/\gamma^* \to \ell^+\ell^-$ data. Jet reconstruction efficiencies and the jet resolutions are adjusted to the values measured in data, and $\not\!\!E_T$ is recalculated accordingly.

Sources of background arise from the production of electroweak bosons that decay into charged leptons. In the ee, $e\mu$, and $\mu\mu$ channels, the dominant backgrounds are Drell-Yan processes: (i) $Z/\gamma^* \to e^+e^-$, (ii) $Z/\gamma^* \to \tau^+\tau^- \to \bar{\nu}\ell^+\nu\nu\ell^-\bar{\nu}$, and (iii) $Z/\gamma^* \to \mu^+\mu^-$, and from diboson production (WW, WZ and ZZ) when the boson decays lead to two charged leptons in the final state. Other backgrounds can be attributed to jets mimicking electrons, muons from semileptonic decays of b quarks, in-flight decays of pions or kaons in a jet, and misreconstructed $\not\!\!E_T$.

The selection efficiencies for the Z/γ^* background are estimated from MC samples generated by ALPGEN interfaced with PYTHIA, while for diboson production they are estimated using PYTHIA. The diboson processes are normalized to the next-to-leading order (NLO) inclusive cross section [36]. The Z/γ^* processes are normalized to the next-to-next-to-leading order (NNLO) inclusive cross section [37] in the $e\mu$ channel. In the other two channels we normalize the MC expectation to the dilepton invariant mass distribution near the Z boson peak. The Z boson p_T distribution predicted by ALPGEN is observed to agree poorly with the data, therefore a reweighting has been performed for samples of different jet multiplicities derived from $Z \to e^+e^-$ data events.

Before making requirements on $\not\!\!E_T$ or its significance, the Z/γ^* background dominates in the ee and $\mu\mu$ channels. Although these events do not contain high-p_T neutrinos, the $Z/\gamma^* \to \ell^+\ell^-$ events can have large $\not\!\!E_T$ from mismeasurement or poor resolution in $\not\!\!E_T$.

Two instrumental backgrounds are modeled using data. In the ee and $e\mu$ channels, background from fake electrons arises from jets comprising an energetic π^0 or η and an overlapping track. The contribution from this source of background is estimated by fitting to the observed distribution of an electron-likelihood discriminant in the data, as described in [31]. The dependence of the electron likelihood is determined for true electrons from a pure Z/γ^* data sample, while the electron likelihood for background is determined using a sample dominated by false electrons. In the $e\mu$ and $\mu\mu$ channels, muons produced in jets that fail to be reconstructed provide muons that appear isolated. We measure the fraction (f_μ) of muons that appear isolated using a dimuon control sample dominated by false isolated muons. The contribution from events with misidentified isolated muons is given by the number of events in a like-sign dilepton sample (without imposing an isolation requirement) multiplied by the measured f_μ defined above.

VI. RECONSTRUCTION OF EVENT KINEMATICS

The calculation of the angular correlation described in Sec. II requires boosting the 4-momenta of the charged leptons back into the t or $\bar{t}$ quark rest frames. Every event must therefore be fully reconstructed. This is performed using the neutrino weighting method, devised originally for measuring m_t in the dilepton channel [38]. The only difference in our procedure is that instead of calculating a weight distribution as a function of the hypothesized m_t, we weight the distribution as a function of $\cos\theta_1 \cos\theta_2$.

In the dilepton final state, the momenta of the two charged leptons, two neutrinos, and two b-quark jets are specified by eighteen components of momentum. We measure twelve of these from the observed leptons and jets. Four additional constraints are provided by requiring the two lepton-neutrino combinations to yield M_W, and the two W-boson+b-jet combinations to yield m_t (which we assume to be 172.5 GeV for t and $\bar{t}$). Two additional quantities must be specified to fully reconstruct the event kinematics.

To obtain the two missing quantities, we sample the pseudorapidity distributions η_1 and η_2 for the two neutrinos into ten bins each using $t\bar{t}$ MC. These distributions are found to be independent of $t\bar{t}$ spin correlation. The bin ranges are chosen in steps of equal probability. We use the median of each bin to resolve the kinematics of the event, with up to two solutions for each of the neutrino transverse momenta.

The measured value of the $\not\!\!E_T$ is then used to assign a weight w to each of the solutions for each assumed set of η values; specifically, for a given η_1 and η_2, we calculate the $\not\!\!E_T$ in the reconstructed event and compare it to the measured $\not\!\!E_T$ as follows:

$$w = \exp\left[-\frac{\left(\not\!\!E_x{}^{calc} - \not\!\!E_x\right)^2 + \left(\not\!\!E_y{}^{calc} - \not\!\!E_y\right)^2}{2\sigma^2_{\not\!\!E_T}}\right], \quad (2)$$

where $\sigma_{\not\!\!E_T}$ is the resolution of the x component of the $\not\!\!E_T$ (taken to be the same as that on the y component) [38]. This assigns a higher weight (w) to $\eta_{1,2}$ pairs that are consistent with the observed $\not\!\!E_T$.

Since it is not possible to unambiguously associate a jet to the correct top quark, all combinations are tried. This increases the possible number of solutions per event from four to eight.

Detector resolutions are accommodated in the weight calculation as follows. For each configuration of a MC event, we simulate the effect of the detector resolution by repeating the calculation 150 times with the measured jet and lepton momenta smeared independently according to the detector response. The resolutions in lepton energies are assumed to be Gaussian and the resolution of the jets is modeled using the sum of two Gaussian distributions [39]. The 150 resolution-smeared weights are averaged, therefore smoothing the weight distribution of an event. This number provides stable and smooth weight distributions, with acceptable computation times. For data, the number of smearings is increased to 1000 to ensure that the result does not depend on statistical fluctuations of the smearing. Events without any solution are ignored in the analysis. The probabilities that the reconstruction of the full event kinematics provides a valid

TABLE 1: Probability that the neutrino weighting procedure yields a valid solution for different classes of events. The $Z \to \tau\tau$, $Z \to \mu\mu$ and $Z \to ee$ backgrounds are shown combined, as are the diboson and instrumental backgrounds. In the last column we give the value observed in data. The statistical uncertainties are $\approx 1\%$.

$t\bar{t}$	Z	Diboson	Instrumental	Total	Observed
0.96	0.82	0.90	0.82	0.92	0.91

solution for $t\bar{t}$ and background events are given in Table 1. Table 2 summarizes the predicted background and the observed number of events in data, together with the number of expected $t\bar{t}$ events using the $t\bar{t}$ cross section measured in this analysis. For each event with a solution the w distribution is normalized to unity, and the mean of the w distribution is used as estimator for the true value of $\cos\theta_1 \cos\theta_2$. The correlation coefficient between our estimator and the true value of $\cos\theta_1 \cos\theta_2$ is about 0.5.

VII. TEMPLATES

Templates of the $\cos\theta_1 \cos\theta_2$ distributions are generated using MC events for different values of C and then compared to data. Figure 2 shows the distribution for $\cos\theta_1 \cos\theta_2$ for background, $t\bar{t}$ signal with NLO QCD spin correlation, and the prediction for $t\bar{t}$ signal without spin correlation. Different fractions of events without and

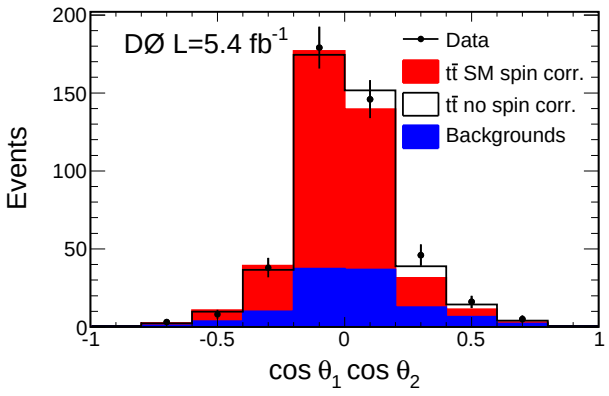

FIG. 2: (Color online) The distribution in $\cos\theta_1 \cos\theta_2$ for the entire dilepton event sample. The summed $t\bar{t}$ signal, including NLO QCD spin correlation ($C = 0.777$) (red) and all backgrounds (blue) are compared to data. The open histogram is the $t\bar{t}$ prediction without spin correlation ($C = 0$). The slight asymmetry in the $\cos\theta_1 \cos\theta_2$ distribution does not bias the measurement.

with SM spin correlation can be used to generate $t\bar{t}$ samples of different true values of C. Templates are formed from the sum of $t\bar{t}$ signals of different C values and contributions from backgrounds, as a function of $\cos\theta_1 \cos\theta_2$. As the ratio of signal to background is different in ee, $e\mu$ and $\mu\mu$ final states, we analyze each channel separately. In each channel, we use eight bins of equal size over the range $[-0.4, 0.4]$, and additionally one bin each for the range $[-1, -0.4]$ and $[0.4, 1]$. The $\cos\theta_1 \cos\theta_2$ distributions in data are compared with these templates to extract the best measured value for C ($C_{\rm meas}$).

VIII. FIT TO TEMPLATES AND SYSTEMATIC UNCERTAINTIES

We perform a binned maximum likelihood fit to extract the measured value $C_{\rm meas}$. We maximize the likelihood function

$$\mathcal{L} = \prod_i \mathcal{P}(n_i, m_i) \times \prod_{k=1}^{K} \mathcal{G}(\nu_k; 0, \mathrm{SD}_k)\,, \qquad (3)$$

where $\mathcal{P}(n, m)$ represents the Poisson probability to observe n events when m events are expected. The first product runs over all the bins i of the templates of all channels. Systematic uncertainties are taken into account by parameters ν_k, where each independent source of systematic uncertainty k is modeled as a Gaussian probability density function, $\mathcal{G}(\nu; 0, \mathrm{SD})$, with zero mean and width corresponding to one standard deviation (SD) in the uncertainty of that parameter. Correlations among systematic uncertainties between channels are taken into account by using the same parameter for the same sources of uncertainty. The predicted number of events in each bin is the sum of the predicted number of background and expected $t\bar{t}$ events and depends on C.

We consider both systematic uncertainties which affect only normalization factors and those which alter the differential distribution of $\cos\theta_1 \cos\theta_2$. Uncertainties derived from differences between data and MC for the jet energy scale, jet energy resolution, jet identification, and from theoretical uncertainties on PDFs, background modeling, and the choice of m_t are taken as differential in $\cos\theta_1 \cos\theta_2$. Systematic uncertainties affecting the overall signal efficiency and the normalization of backgrounds include lepton identification, trigger requirements, uncertainties on the normalization of background, the uncertainty on the luminosity, MC modeling, and the determination of instrumental background. We also include an uncertainty on the templates because of limited statistics in the MC samples. We estimate the latter from 1000 pseudo-experiments, where we randomly vary each bin in the templates within the statistical uncertainty of the MC and repeat the measurement on data.

The statistical and systematic uncertainties on $C_{\rm meas}$ are listed in Table 3. We evaluate the size of the individual sources of systematic uncertainty by setting all parameters for the systematic uncertainties to their fitted mean value and calculate the impact of the upward and downward one standard deviation uncertainty on the

TABLE 2: Yields for events with a solution in the neutrino weighting procedure. The number of $t\bar{t}$ events is calculated using $\sigma_{t\bar{t}} = 7.92$ pb as measured in this analysis. The $Z \to \tau\tau$, $Z \to \mu\mu$, and $Z \to ee$ backgrounds are shown combined, as are the different instrumental backgrounds. Uncertainties include statistical and systematic contributions.

	$t\bar{t}$	Z	Diboson	Instrumental	Expected	Observed
Number of events	324^{+28}_{-28}	75^{+13}_{-13}	17^{+3}_{-3}	23^{+4}_{-4}	439^{+36}_{-36}	441

fitted parameter on the measured quantities $C_{\rm meas}$ and $\sigma_{t\bar{t}}$.

IX. RESULT

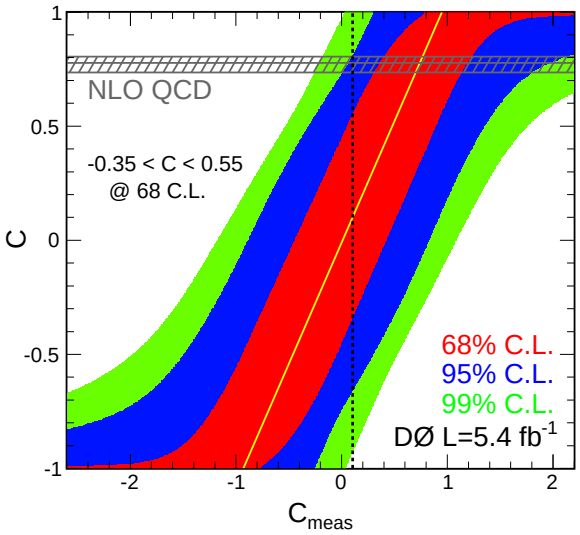

FIG. 3: (Color online) The 68% (inner), 95% (middle), and 99% (outer) C.L. bands of C as a function of $C_{\rm meas}$ from likelihood fits to MC events for all channels combined. The yellow line indicates the most probable value of C as a function of $C_{\rm meas}$, and represents the calibration of the method. The vertical dashed black line depicts the measured value $C_{\rm meas} = 0.10$. The horizontal band indicates the NLO QCD prediction of $C = 0.777^{+0.027}_{-0.042}$.

To estimate the expected uncertainty of the result, ensembles of MC experiments are generated for different values of C, and the maximum likelihood fit is repeated, yielding a distribution of $C_{\rm meas}$ for each C. Systematic uncertainties are included in this procedure, taking into account correlations between channels. We then apply the "ordering principle" for ratios of likelihoods [40] to the MC distributions of $C_{\rm meas}$ and generated C. Due to fluctuations in the data the best fit value for $C_{\rm meas}$ can lie outside the physical region, however, a physically meaningful value for C can be extracted for any value of $C_{\rm meas}$ by using Fig. 3. For the SM expectation of $C = 0.777$ we expect to exclude values below -0.06 at the 95% C.L. From the maximum likelihood fit to data we obtain $C_{\rm meas} = 0.10^{+0.42}_{-0.44}\,({\rm stat+syst})$, which is shown in Fig. 3. We transform $C_{\rm meas}$ into

$$C = 0.10^{+0.45}_{-0.45}\,({\rm stat+syst})\ , \qquad (4)$$

and extract a 95% C.L. region of probability for C as $[-0.66, 0.81]$. Our result is within two standard deviations of the NLO QCD prediction of $C = 0.777^{+0.027}_{-0.042}$ but also compatible with the no-correlation hypothesis.

The simultaneously extracted $t\bar{t}$ cross section is found to be

$$\sigma_{t\bar{t}} = 7.92^{+1.07}_{-0.93}\,({\rm stat\ +\ syst})\ \ {\rm pb} \qquad (5)$$

for $m_t = 172.5$ GeV, which agrees with the SM prediction of $\sigma_{t\bar{t}} = 7.46^{+0.48}_{-0.67}$ pb [16].

X. CONCLUSION

We have measured the spin correlation between top and anti-top quarks in $t\bar{t}$ production using a differential angular distribution in lepton decay angles. The correlation coefficient characterizing the degree of spin correlation is found to be $C = 0.10^{+0.45}_{-0.45}$. This is the most precise result obtained from the analysis of top quark pair production in dilepton final states. Since the measured value of C agrees with the SM prediction of $C = 0.777^{+0.027}_{-0.042}$ in NLO QCD within two standard deviations, there is no significant hint for anomalous production or decay of top quark pairs.

Acknowledgments

We wish to thank W. Bernreuther, S. J. Parke, and P. Uwer for fruitful discussions regarding this analysis. We thank the staffs at Fermilab and collaborating institutions, and acknowledge support from the DOE and NSF (USA); CEA and CNRS/IN2P3 (France); FASI, Rosatom and RFBR (Russia); CNPq, FAPERJ, FAPESP and FUNDUNESP (Brazil); DAE and DST (India); Colciencias (Colombia); CONACyT (Mexico); KRF and KOSEF (Korea); CONICET and UBACyT (Argentina); FOM (The Netherlands); STFC and the Royal Society (United Kingdom); MSMT and GACR (Czech

TABLE 3: Summary of uncertainties on $C_{\rm meas}$.

Source	+SD	−SD
Muon identification	0.01	−0.01
Electron identification and smearing	0.01	−0.01
PDF	0.02	−0.01
Top Mass	0.01	−0.01
Triggers	0.02	−0.02
Opposite charge requirement	0.00	−0.00
Jet energy scale	0.01	−0.01
Jet reconstruction and identification	0.06	−0.06
Normalization	0.02	−0.02
Monte Carlo statistics	0.02	−0.02
Instrumental background	0.00	−0.00
Background Model for Spin	0.03	−0.04
Luminosity	0.03	−0.03
Other	0.01	−0.01
Template statistics for template fits	0.07	−0.07
Total systematic uncertainty	0.11	−0.11
Statistical uncertainty	0.38	−0.40

Republic); CRC Program and NSERC (Canada); BMBF and DFG (Germany); SFI (Ireland); The Swedish Research Council (Sweden); and CAS and CNSF (China).

[1] V. D. Barger, J. Ohnemus, and R. J. N. Phillips, Int. J. Mod. Phys. A **4**, 617 (1989).

[2] I. I. Y. Bigi, Y. L. Dokshitzer, V. A. Khoze, J. H. Kühn, and P. M. Zerwas, Phys. Lett. B **181**, 157 (1986).

[3] A. F. Falk and M. E. Peskin, Phys. Rev. D **49**, 3320 (1994).

[4] A. Brandenburg, Z. G. Si, and P. Uwer, Phys. Lett. B **539**, 235 (2002).

[5] W. Bernreuther, A. Brandenburg, Z. G. Si and P. Uwer, Nucl. Phys. B **690**, 81 (2004).

[6] T. Stelzer and S. Willenbrock, Phys. Lett. B **374**, 169 (1996).

[7] W. Bernreuther, M. Flesch and P. Haberl, Phys. Rev. D **58**, 114031 (1998).

[8] I. I. Y. Bigi, Phys. Lett. B **175**, 233 (1986).

[9] M. Jezabek and J. H. Kühn, Phys. Lett. B **329**, 317 (1994).

[10] G. R. Goldstein, K. Sliwa, and R. H. Dalitz, Phys. Rev. D **47**, 967 (1993).

[11] W. Bernreuther, M. Fücker, and Y. Umeda, Phys. Lett. B **582**, 32 (2004).

[12] T. Aaltonen *et al.* [CDF Collaboration], Phys. Rev. D **83**, 031104 (2011).

[13] B. Abbott *et al.* [D0 Collaboration], Phys. Rev. Lett. **85**, 256 (2000).

[14] We follow the convention in Ref. [5].

[15] V. Ahrens *et al.*, J. High Energy Phys. **09**, 097 (2010); V. Ahrens *et al.*, Nucl. Phys. Proc. Suppl. **205-206**, 48 (2010).

[16] S. Moch and P. Uwer, Phys. Rev. D **78**, 034003 (2008); U. Langenfeld, S. Moch, and P. Uwer, Phys. Rev. D **80**, 054009 (2009); M. Aliev *et al.*, Comput. Phys. Commun. **182**, 1034 (2011).

[17] N. Kidonakis and R. Vogt, Phys. Rev. D **68**, 114014 (2003).

[18] N. Kidonakis, Phys. Rev. D **82**, 114030 (2010).

[19] M. Cacciari *et al.*, J. High Energy Phys. **04**, 068 (2004).

[20] P. Fayet and S. Ferrara, Phys. Rept. **32**, 249 (1977).

[21] V. M. Abazov *et al.* [D0 Collaboration], Phys. Lett. B **696**, 321 (2011).

[22] Here the t and $\bar{t}$ quark rest frames are obtained by first boosting into the $t\bar{t}$ zero mass frame. If the t and $\bar{t}$ quark rest frames were constructed by directly boosting from the laboratory frame, a Wigner rotation would have to be taken into account.

[23] S. Frixione and B. R. Webber, J. High Energy Phys. **06**, 029 (2002).

[24] V. M. Abazov *et al.* [D0 Collaboration], Nucl. Instrum. Methods Phys. Res. A **565**, 463 (2006); M. Abolins *et al.*, Nucl. Instrum. Methods Phys. Res. A **584**, 75 (2008); R. Angstadt *et al.*, Nucl. Instrum. Methods Phys. Res. A **622**, 298 (2010).

[25] The rapidity y and pseudorapidity η of a particle are defined as functions of the polar angle θ and velocity parameter β as $y(\theta,\beta) \equiv \frac{1}{2}\ln\left[(1+\beta\cos\theta)/(1-\beta\cos\theta)\right]$ and $\eta(\theta) \equiv y(\theta,1)$, where β is the ratio of a particle's momentum to its energy. We distinguish detector η ($\eta_{\rm det}$) and collision η, where the former is defined with respect to the center of the detector and the latter with respect to the $p\bar{p}$ interaction vertex.

[26] The impact parameter is defined as the distance of closest approach (d_{ca}) of the track to the PV in the plane transverse to the beamline. The impact parameter significance is defined as $d_{ca}/\sigma_{d_{ca}}$, where $\sigma_{d_{ca}}$ is the uncertainty on

d_{ca}.
[27] V. M. Abazov *et al.*, Nucl. Instrum. Meth. A **552**, 372 (2005).
[28] V. M. Abazov *et al.* [D0 Collaboration], Phys. Rev. D **76**, 092007 (2007).
[29] V. M. Abazov *et al.* [D0 Collaboration], Phys. Lett. B **679**, 177 (2009).
[30] G. C. Blazey *et al.*, arXiv:hep-ex/0005012 (2000).
[31] V. M. Abazov *et al.* [D0 Collaboration], Phys. Rev. D **76**, 052006 (2007).
[32] G. Corcella *et al.*, J. High Energy Phys. **01**, 010 (2001).
[33] M. L. Mangano *et al.*, J. High Energy Phys. **07**, 001 (2003). We use ALPGEN version 2.11.
[34] T. Sjöstrand *et al.*, Comp. Phys. Commun. **135**, 238 (2001). We use PYTHIA version 6.409.
[35] R. Brun and F. Carminati, CERN Program Library Long Writeup W5013, 1993 (unpublished).
[36] J.M. Campbell and R.K. Ellis, Phys. Rev. D **60**, 113006 (1999).
[37] R. Hamberg, W. L. van Neerven, T. Matsuura, Nucl. Phys. **B359**, 343-405 (1991) [Erratum-ibid. B **644**, 403 (2002)].
[38] V. M. Abazov *et al.* [D0 Collaboration], Phys. Rev. D **80**, 092006 (2009); B. Abbott *et al.* [D0 Collaboration], Phys. Rev. Lett. **80**, 2063 (1998).
[39] A. Grohsjean, Fermilab-Thesis-2008-92 (2008).
[40] G. J. Feldman and R. D. Cousins, Phys. Rev. D **57**, 3873 (1998).